PCCP

PAPER

View Article Online
View Journal | View Issue

Cite this: *Phys. Chem. Chem. Phys.*, 2018, **20**, 15995

Supramolecular multicompartment gels formed by ABC graft copolymers: high toughness and recovery properties†

Pengxiang Xu, Jiaping Lin * and Liangshun Zhang *

Received 31st March 2018,
Accepted 8th May 2018

DOI: 10.1039/c8cp02062k

rsc.li/pccp

We conceptually design multicompartment gels with supramolecular characteristics by taking advantage of amphiphilic ABC graft copolymers. The ABC graft copolymers contain a solvophilic **A** backbone and solvophobic **B** and **C** grafts, where the **C** grafts interact with each other *via* hydrogen bonds. The mechanical properties of supramolecular multicompartment gels under uniaxial tension are studied by coupling dissipative particle dynamics simulations with the nonequilibrium deformation technique. The results show that the supramolecular multicompartment gels exhibit high toughness and recovery properties, while their stiffness is maintained. Due to the physical origin, the superior mechanical properties of supramolecular gels have a tight relation with the structural relaxation of grafts and the association–disassociation dynamics of hydrogen bonds. In addition, the toughness of the multicompartment gels can be further tuned by adjusting the strength and directivity of the hydrogen bonds. The present work unveils the physical origin of the distinct mechanical properties of supramolecular gels, which may provide useful guidance for designing functional gels with superior toughness.

Introduction

Supramolecular gels are among the most attractive soft materials due to their widespread applications in the fields of artificial tissues, drug delivery, and shape-memory materials.[1–3] Investigations on the gel structure, gelation mechanism, and mechanical properties of supramolecular gels are essential from the viewpoints of both theoretical research and engineering applications.[4–6] Supramolecular gels are generally formed by physically cross-linking networks of building blocks, which are held together by non-covalent interactions, such as solvophobic interactions, π–π stacking, metal coordination, or hydrogen bonding.[5] In a specific time scale, the supramolecular network is living and transient, *i.e.*, the network structure can continuously change because the non-covalent interactions have the capability to be dynamically broken and reformed.[7] As a result, the supramolecular gels associated by non-covalent interactions generally exhibit stimuli-response and self-healing properties upon exposure to an external stimulus.[8–10]

Recently, many researchers have reported superior mechanical properties of supramolecular gels cross-linked by reversible hydrogen bonding groups.[11–16] For example, Gong and co-authors investigated the structure and mechanical properties of a blend system consisting of poly(dodecyl glyceryl itaconate) (PDGI) and polyacrylamide (PAAm).[15] By association of the hydrogen bonding between PDGI and PAAm, the blend forms supramolecular hydrogels with a strong tensile strength and self-healing properties. Some researchers found that the mechanical properties of supramolecular gels containing multivalent hydrogen bonding groups, such as ureidopyrimidinone (UPy) groups, are more excellent than those cross-linked by monovalent groups.[17–20] Note that the association between the UPy group and H_2O has an inverse effect on the mechanical properties of supramolecular gels. To prevent the formation of UPy–H_2O hydrogen bonds, the hydrophobic UPy-based polymers are covalently linked by hydrophilic polymers, such as poly(2-(*N*,*N*-dimethylamino)ethyl methacrylate) or poly(ethylene glycol).[14,21] In these amphiphilic copolymers, the UPy–UPy dimers are embedded in hydrophobic domains, which are physically cross-linked by longer hydrophilic blocks. The supramolecular hydrogels of the amphiphilic copolymers present superior toughness and strong stretchability.

In the supramolecular gels of amphiphilic copolymers, the competition between the self-assembly of macromolecular compounds and the association–disassociation behaviors of hydrogen bonds leads to the complex dynamics of gels.[22,23] Rubinstein *et al.* have developed a theory to investigate the dynamics of associating polymers which consist of a soluble backbone and associating stickers.[23] It was found that the lifetime

Shanghai Key Laboratory of Advanced Polymeric Materials, State Key Laboratory of Bioreactor Engineering, Key Laboratory for Ultrafine Materials of Ministry of Education, School of Materials Science and Engineering, East China University of Science and Technology, Shanghai 200237, China. E-mail: jlin@ecust.edu.cn, zhangls@ecust.edu.cn

† Electronic supplementary information (ESI) available. See DOI: 10.1039/c8cp02062k

of hydrogen bonds and the Rouse relaxation time of stickers play a vital role in the dynamics of the associating polymers. Besides the theoretical studies, many experimental efforts have been devoted to investigating the influence of hydrogen bonding groups on the dynamics and rheological properties of supramolecular gels.[24–28] However, the uniaxial tension behaviors of supramolecular gels are less a concern and the relationship between the tensile behaviors and the microscopic information on the gel network is still poorly understood.

Apart from the experiments, theoretical simulation methods, such as self-consistent field theory,[29,30] molecular dynamics (MD),[31–37] Monte-Carlo (MC) simulation,[38–41] and dissipative particle dynamics (DPD)[42–47] are useful tools to investigate the mechanical properties of supramolecular gels. For example, Baljon and co-authors utilized hybrid MD and MC simulations to study the shear rheological properties of self-associating polymer networks.[40] It was found that the rheological properties are correlated with the network structure as well as the balance between the breaking and reforming of structural elements. Yan's group employed DPD simulations to study the mechanical properties of associating polymers grafted on Janus nanoparticles.[48] It was revealed that the stiffness and spatial organization of polymer chains can regulate the reactivity of polymers and affect their self-healing capabilities. Xu *et al.* adopted nonequilibrium DPD simulations to study the rheological properties of rod-coil amphiphilic copolymer gels.[49] It was found that the flow curve displays distinct three-regime flow behaviors. However, there exist only limited theoretical studies on the mechanical properties of supramolecular gels under uniaxial tension. Many important issues, such as the stress–strain relation, the hydrogen bond dynamics and the dynamics of structural relaxation remain to be further studied. The success of the nonequilibrium DPD method makes it capable of exploring the dynamics and the mechanical properties of supramolecular gels.

It should be pointed out that the previous simulations mentioned above ignore the directivity of hydrogen bonds. In the actual system of polymers, the hydrogen bonds are formed only when the angle among the donor atom, hydrogen and the acceptor atom is of a limited value. It was experimentally demonstrated that the directivity of hydrogen bonds plays an important role in determining the structures and mechanical properties of supramolecular gels.[24] To explore the effect of hydrogen bonds on the mechanical properties of gels, the directivity of hydrogen bonds in our model is introduced through a directional dependence force field, such as the DREIDING force field.[50]

In this work, by introducing hydrogen bonds to the **C** grafts of ABC graft copolymers, we conceptually designed supramolecular multicompartment gels, where the **B** and **C** grafts form solvophobic domains physically linked by the chains of the **A** backbone. With the help of DPD simulations and the nonequilibrium deformation technique, we investigated the mechanical properties and recovery properties of supra-molecular multicompartment gels under uniaxial tension. The effects of polymer concentration and the strength and directivity of hydrogen bonds on the mechanical properties were examined. More importantly, the Rouse relaxation dynamics of grafts and the association–disassociation dynamics of hydrogen bonds were analyzed to reveal the relationship between the mechanical properties and the microscopic information of gel networks.

Methods and model

In the DPD, polymer molecules are modelled by bead-spring chains. All beads having a mass of m represent a cluster of atoms and interact pairwise *via* bead–bead interactions. The force $\mathbf{f}_i$ acting on ith bead includes the conservative force $\mathbf{F}_{ij}^{C}$, the dissipative force $\mathbf{F}_{ij}^{D}$, and the random force $\mathbf{F}_{ij}^{R}$, given by[51]

$$\mathbf{f}_i = \sum_{j \neq i} \left(\mathbf{F}_{ij}^{C} + \mathbf{F}_{ij}^{D} + \mathbf{F}_{ij}^{R} \right) \quad (1)$$

The conservative force is a soft repulsion taking the form of $\mathbf{F}_{ij}^{C} = a_{ij}\omega^{0.5}(r_{ij})\hat{\mathbf{r}}_{ij}$, where a_{ij} is the repulsive parameter between the ith and jth beads. $\mathbf{r}_i$ is the position of the i-th bead, $\mathbf{r}_{ij} = \mathbf{r}_i - \mathbf{r}_j$, $r_{ij} = |\mathbf{r}_{ij}|$, and $\hat{\mathbf{r}}_{ij} = \mathbf{r}_{ij}/r_{ij}$. The weight function $\omega(r_{ij})$ is set as $(1 - r_{ij}/r_c)^2$ within a cutoff distance r_c and vanishes beyond r_c.[51] The dissipative force is $\mathbf{F}_{ij}^{D} = -\gamma\omega(r_{ij})(\hat{\mathbf{r}}_{ij}\cdot\mathbf{v}_{ij})\hat{\mathbf{r}}_{ij}$ where γ is the friction coefficient, $\mathbf{v}_i$ is the velocity of i-th bead, and $\mathbf{v}_{ij} = \mathbf{v}_i - \mathbf{v}_j$. The random force is given by $\mathbf{F}_{ij}^{R} = \Gamma\omega^{0.5}(r_{ij})\theta_{ij}\hat{\mathbf{r}}_{ij}$, where θ_{ij} is the Gaussian white noise and Γ is the noise amplitude. Γ and γ satisfy the fluctuation-dissipative theorem as $\Gamma^2 = 2\gamma k_B T$, where $k_B T$ is the thermal energy. In the simulations, reduced units are adopted for all physical quantities.[51] The units of mass, length, and energy are m, r_c, and $k_B T$, respectively. The time unit τ can be obtained by $\tau = (m r_c^2/k_B T)^{1/2}$, and its real value can be estimated by matching the simulated lateral diffusion coefficient to the experiment measured value.[51]

As shown in Fig. 1, each ABC graft copolymer consists of a flexible **A** backbone grafted by flexible **B** and **C** blocks. The grafts, including two **B** blocks and two **C** blocks, are symmetrically and uniformly attached onto the **A** backbone. The position of the first graft point (denoted by s_1) is defined as the length ratio of the free end block (L_1) to the backbone (L_b), $s_1 = L_1/L_b$. The backbone and each graft respectively contain 51 and 3 beads, and the s_1 is fixed at 0.02. The design of this molecular architecture, *i.e.*, the length of

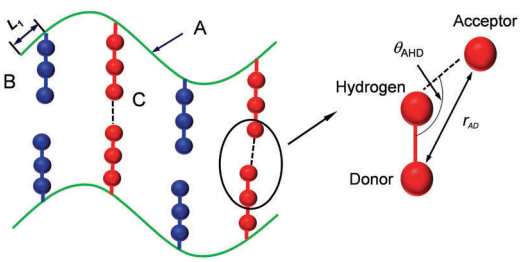

Fig. 1 DPD model of ABC graft copolymers. Each chain consists of a solvophilic **A** backbone and solvophobic grafts including two **B** grafts and two **C** grafts. The length of the free end block of the backbone is denoted by L_1. The **C** grafts interact with each other *via* hydrogen bonds. The enlarged view shows the hydrogen bonding interaction described by the 3-body acceptor–hydrogen–donor potential. θ_{AHD} is the angle among the donor, hydrogen, and acceptor beads, and r_{AD} is the radial distance between the donor and acceptor beads.

backbone is much longer than that of grafts, is motivated by the experimental system reported by Anthamatten's group.[52]

In polymer chains, neighboring beads are connected by a harmonic spring force $\mathbf{F}_{ij}^{S} = k_c(r_{ij} - r_{eq})\hat{\mathbf{r}}_{ij}$, where the spring constant is $k_c = 100.0k_BT/r_c^2$, and the equilibrium length is $r_{eq} = 0.85r_c$. The **A** backbone is chosen to be solvophilic, while the **B** and **C** grafts are chosen to be solvophobic. The repulsive parameters between different types of beads are $a_{AB} = a_{AC} = 60.0k_BT/r_c^2$, $a_{BC} = a_{BS} = a_{CS} = 80.0k_BT/r_c^2$, and $a_{AS} = 15.0k_BT/r_c^2$, where the subscripts A, B, C, and S denote the beads of **A**, **B**, **C**, and the solvent, respectively. The repulsive parameters between the same types of beads are $25.0k_BT/r_c^2$. The solubility of **B** and **C** grafts is identical, except that the **C** grafts interact with each other *via* hydrogen bonds.

The hydrogen bonds between **C** grafts are described by the acceptor–hydrogen–donor (AHD) 3-body interaction potential based on the DREIDING force field[50,53]

$$U^{hb}(r_{AD}) = \begin{cases} k_A\left(20r_{AD}^{-12} - 24r_{AD}^{-10}\right)\cos^4\theta & \text{for } r_{AD} < R_c \text{ and } \theta_{AHD} > \theta_c \\ 0 & \text{else} \end{cases} \quad (2)$$

where k_A, R_c, and θ_c are the force constant, cutoff distance, and cutoff angle, respectively. θ_{AHD} is the bond angle among the hydrogen acceptor (A), hydrogen (H), and hydrogen donor (D), while r_{AD} is the radial distance between the donor and acceptor (Fig. 1). The hydrogen bonding interaction between a pair of **C** grafts exists only when the r_{AD} is within the cutoff distance R_c and the θ_{AHD} is larger than the cutoff angle θ_c. Otherwise, the hydrogen bonding interaction vanishes. Therefore, the hydrogen bonds described by the AHD potential are reversible due to their dynamical breaking and reforming. More importantly, directivity is introduced into the hydrogen bonds formed only in a limited range.

An initial cubic box of $30 \times 30 \times 30\ r_c^3$ with periodic boundary conditions was adopted by using the large atomic/molecular massively parallel simulator (LAMMPS).[54] 81 000 DPD beads with a polymer concentration of ϕ were randomly generated in the cubic box. Herein, ϕ is defined as the ratio of the polymer bead amount to the total bead amount. After construction of the initial configurations, standard DPD simulations were performed in an *NVT* ensemble with $k_BT = 1.0$ by using the Nose–Hoover thermostat.[51] The velocity-Verlet algorithm was adopted for 6×10^5 steps with a time-step of $\Delta t = 0.01\tau$. After that, to investigate the mechanical properties, uniaxial tensile simulations were carried out by deforming the cubic box to a rectangular one.[55,56] The box is elongated in the *x*-direction and compressed in the *y*-direction and the *z*-direction, while the box volume remains invariable. Therefore, the Poisson ratio is $\mu = 0.5$, which is close to that of rubbery materials. The tensile strain ε is the elongation in the *x*-direction Δx divided by the box edge length L_x (*i.e.*, $\varepsilon = \Delta x/L_x$), and the strain rate is the time derivative of the tensile strain. The tensile stress σ_x in the *x*-direction is calculated by the deviatoric part of the stress tensor[57]

$$\sigma_x = (1 + \mu)(\sigma_{xx} + P) = 3(\sigma_{xx} + P)/2 \quad (3)$$

where $P = \sum_{\alpha} P_{\alpha\alpha}/3$ is the hydrostatic pressure. The diagonal component $P_{\alpha\alpha}$ of the pressure tensor is the negative value of virial stress $\sigma_{\alpha\alpha}$ in the α-direction calculated by the tensor version of the virial theorem

$$\sigma = \frac{1}{V}\left\langle \sum_i m_i \mathbf{v}_i \mathbf{v}_i + \frac{1}{2}\sum_{i \neq j} \mathbf{r}_{ij} \cdot \mathbf{F}_{ij} \right\rangle \quad (4)$$

where V denotes the volume of the system and the angular bracket represents the ensemble average. To eliminate the internal stress, the initial stress $\sigma_{x,0}$ is subtracted from the tensile stress σ_x. Note that for a given parameter setting, 5 tensile tests were performed for an ensemble average of stress.

Results and discussion

In the present work, we focused on the mechanical properties of supramolecular multicompartment gels formed by ABC graft copolymers. First, we investigated the effect of polymer concentration on the mechanical properties of ABC copolymer gels. Then, the microscopic origin of the distinct mechanical properties was examined by analyzing the Rouse relaxation behaviors of the graft chains and the association–disassociation dynamics of hydrogen bonds. Finally, the mechanical properties of supramolecular multicompartment gels are studied by tuning the strength and directivity of hydrogen bonding interactions.

Effect of polymer concentration on mechanical properties

In this subsection, DPD simulations of ABC graft copolymer solutions with various polymer concentrations ϕ were performed to investigate their equilibrium structures and mechanical properties. The force constant k_A, cutoff distance R_c, and cutoff angle θ_c of the AHD potential (see eqn (2)) for hydrogen bonds between **C** blocks are fixed at $5.0k_BT$, $2.5r_c$, and 150°, respectively. As shown in Fig. S1a and b of the ESI,† the ABC graft copolymers in solutions with $\phi = 0.10$ and $\phi = 0.40$ self-assemble into micelles and multicompartment gels, respectively. In the gels, the solvophobic **B** and **C** grafts are segregated into different domains, which are physically connected by the solvophilic **A** backbones. It should be pointed out that the density of the gel network can be regulated by the distance between the grafts along the **A** backbone (*i.e.*, the length of bridging subchains). The subchains of the backbone adopt a bridging or dangling conformation. Only the bridging subchains contribute to the gel network. As the position s_1 of the first graft point decreases, the length ratio of the bridging subchains to the dangling subchains increases, resulting in an increase of gel density. For comparison, the equilibrium structures of ABC graft copolymer solutions without hydrogen bonds were also examined (see Fig. S1c and d of ESI†). The systems with and without hydrogen bonds self-assemble into similar structures at the same polymer concentrations.

Fig. 2a shows the stress–strain curves of ABC copolymer solutions with various ϕ under uniaxial tension of a constant tensile rate of $0.2\tau^{-1}$. The tensile rate is chosen on the basis of the reciprocal of the segmental relaxation time of the polymer

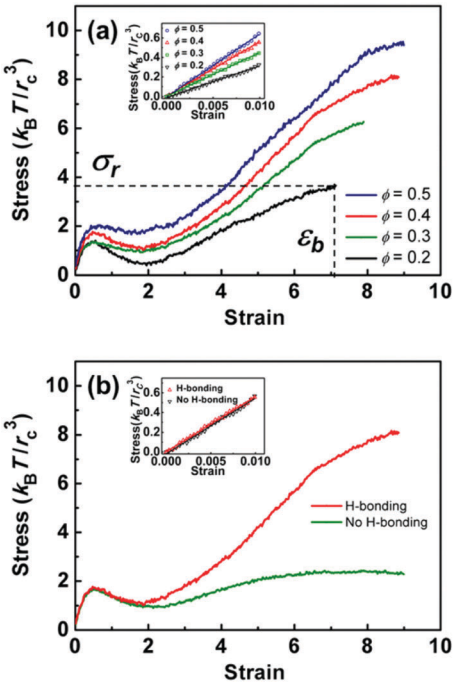

Fig. 2 (a) Stress–strain curves of ABC graft copolymer solutions with various polymer concentrations ϕ. The rupture stress σ_r and the elongation at break ε_b are highlighted in the plot. (b) Stress–strain curves of ABC copolymer gels with and without hydrogen bonding interactions for ϕ = 0.40. The insets are the stress–strain behavior at small tensile strains of $\varepsilon < 0.01$.

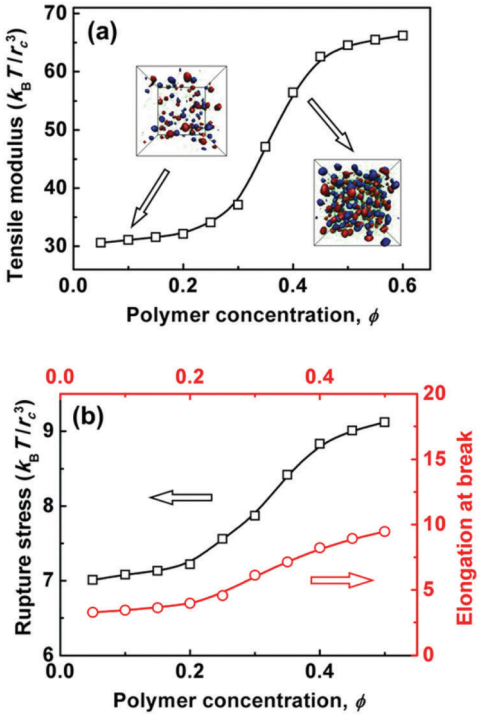

Fig. 3 (a) Tensile modulus E as a function of ϕ for ABC graft copolymer solutions. The insets show the structural snapshots of the systems with ϕ = 0.10 and ϕ = 0.40 at the equilibrium state. (b) Rupture stress (black) and elongation at break (red) as a function of ϕ for ABC graft copolymer solutions. The tensile rate is fixed at $0.2\tau^{-1}$.

chains, which is on a scale of 5–10τ according to the work of Gao and Weiner.[58] As the tensile strain increases, the stress gradually increases due to the elastic deformation at small strain ($\varepsilon < 0.5$), followed by a decrease (stress softening) at intermediate strain ($0.5 < \varepsilon < 2.0$). Finally, the stress increases (strain hardening) again with further increasing of the tensile strain ($\varepsilon > 2.0$). The stress data are not presented after the fracture of samples. The stress–strain relationship is in accordance with the observations on common supramolecular hydrogels in experiments.[14,28,59]

For comparison, the uniaxial tension behaviors of ABC graft copolymer gels without hydrogen bonding interactions were also examined. Fig. 2b shows the stress–strain curves of the systems with and without hydrogen bonds between **C** grafts. The polymer concentration is fixed at ϕ = 0.40, and the tensile rate is fixed at $0.2\tau^{-1}$. From the comparison between these two systems, one can deduce that the hydrogen bonds enhance the stress at larger strains, while having a weak influence on the stress at smaller strain. This phenomenon manifests the fact that the hydrogen bonds enhance the toughness of gels, while maintaining the stiffness.

From the inset of Fig. 2a, it can be seen that the stress is proportional to the strain in the small-strain-regime of $\varepsilon < 0.01$. The tensile modulus E is deduced through linear fitting of the stress–strain data in this regime. For instance, the tensile moduli of systems with ϕ = 0.20, ϕ = 0.30, ϕ = 0.40, and ϕ = 0.50 are $32.12k_BT/r_c^3$, $37.45k_BT/r_c^3$, $56.41k_BT/r_c^3$, and $64.52k_BT/r_c^3$, respectively. Fig. 3a shows the tensile moduli E as a function of the polymer concentration ϕ. With increasing ϕ, the E gradually increases, suggesting that the stiffness of the gel systems is enhanced. Note that the E increases sharply around ϕ = 0.35, which qualitatively corresponds to the critical point of sol–gel transition in the experiments.[6] The structural snapshots for the samples with ϕ = 0.10 and ϕ = 0.40 are shown in the insets of Fig. 3a. When the ϕ is lower than the critical point (*e.g.*, ϕ = 0.10), the **B**- and **C**-rich solvophobic domains are separated by a long distance, and thus the solvophilic **A** backbones cover the solvophobic domains in a frustrated way. These phenomena result in the formation of isolated micelles with a lower tensile modulus. When the ϕ is larger than the critical point (*e.g.*, ϕ = 0.40), more solvophobic domains are formed and become close. Consequently, the solvophilic **A** backbones connect the solvophobic domains to form the gel networks, leading to an sharp increase of tensile modulus.

We then paid attention to the stress–strain relationships in the non-linear regime of $\varepsilon \geq 0.5$. The multicompartment gels of ABC graft copolymers exhibit a yield behavior of around ε = 0.5, *i.e.*, the stress reaches a maximum value (Fig. 2a), which is in line with the stress overshoot phenomenon in the experiments.[27] The yield stress is the stress at the yield point which indicates the limit of elastic deformation and the beginning of the plastic deformation. As the ϕ increases, the density of the gel network increases, and thus the elastic properties are enhanced, leading to the increase of yield stress (Fig. 2a). When $\varepsilon > 0.5$, the samples exhibit stress softening at $0.5 < \varepsilon < 2.0$, followed by

strain hardening at $\varepsilon > 2.0$. The stress softening could be related to the segmental re-arrangement caused by structural relaxation of the solvophobic domain, disassociation and re-association of hydrogen bonds, and the slippage of polymers. With increasing ϕ, the density gel of the network increases and the gels become harder and stronger. As a result, the segmental re-arrangement is more difficult to take place for larger ϕ, and the stress softening is weaker. At a larger strain, the samples are fractured, where the stress and strain respectively correspond to the rupture stress σ_r and the elongation at break ε_b. The dependence of ε_b and σ_r on the ϕ is shown in Fig. 3b. It can be seen that both the ε_b and the σ_r increase with increasing the ϕ, suggesting that the toughness of gels is enhanced in the system with a larger ϕ.

Physical origin of distinct mechanical properties

The high toughness of supramolecular gels could originate from the dissipation of energy, which has a tight relation with the structural relaxation of solvophobic domains as well as the disassociation and re-association behaviors of hydrogen bonds. To verify the influences of these two factors on the mechanical properties, we monitored the structural relaxation of solvophobic domains and the association–disassociation dynamics of hydrogen bonds. Taking the gel system with $\phi = 0.40$ as an example, we examined the evolution of the aggregate structure and hydrogen bonds in the elongation process.

During the elongation, structural relaxation takes place as the solvophobic domains transform from spheres to rods (see Fig. 4a). To get a deeper insight into the structural relaxation of the solvophobic domains, we introduce the average bond length $\langle l_b \rangle$ and the bond orientation parameter $\langle p_2 \rangle$ to characterize the conformational changes of **B** and **C** grafts. The $\langle l_b \rangle$ is defined as the average distance of neighbor beads in the grafts, characterizing the stretching degree of bonds. The $\langle p_2 \rangle$, given by $(3\langle \cos^2\theta \rangle - 1)/2$, represents the orientation degree of grafts. As shown in the inset of Fig. 4c, θ is denoted as the angle between the bond and the tensile direction. Fig. 4b and c depict the $\langle l_b \rangle$ and $\langle p_2 \rangle$ as a function of the strain, respectively. During the elongation process, the $\langle l_b \rangle$ slightly grows, and at the same time the $\langle p_2 \rangle$ rapidly grows, indicating that the graft chains are gradually orientated along the tensile direction with slight stretching. The orientation behavior leads to the slippage of grafts, which is in accordance with the chain pulling-out mode of physically linked networks.[60] As a result, the structural relaxation takes place, leading to the energy dissipation. The systems with various concentrations ϕ were also examined. It was found that the samples with different ϕ show similar behaviors of structural relaxations (*i.e.*, the solvophobic domains transform from spheres to rods), and both the $\langle p_2 \rangle$ and $\langle l_b \rangle$ gradually increase during the elongation process.

In addition to the orientation behavior of single bonds, we also examined the orientation of grafts in the scale of a single polymer chain. The orientation degree $\langle p_g \rangle$ of grafts is given by $(3\langle \cos\theta_g \rangle - 1)/2$, where θ_g is the angle between the tensile direction and the end-to-end vector of grafts (see the inset of Fig. S2 of ESI†). Similar to the evolution of $\langle l_b \rangle$ and $\langle p_2 \rangle$, the value of $\langle p_g \rangle$ gradually increases in the elongation process (see Fig. S2 of ESI†), further indicating that the grafts are gradually orientated along the tensile direction. The orientation of the grafts leads to the deformation of the gel network.

We then examined the type of deformation (*i.e.* affine or non-affine deformation) of the gels by tracking the positions of randomly picked tracer beads in the elongation process. Affine deformation implies that the local strain is uniformly distributed and identical to the global macroscopic strain. Fig. S3a of ESI† shows the x-component r_x of the position vector of six tracer beads. It can be seen that the beads with the same r_x at initial state (such as the 120-th and 356-th beads) have different r_x

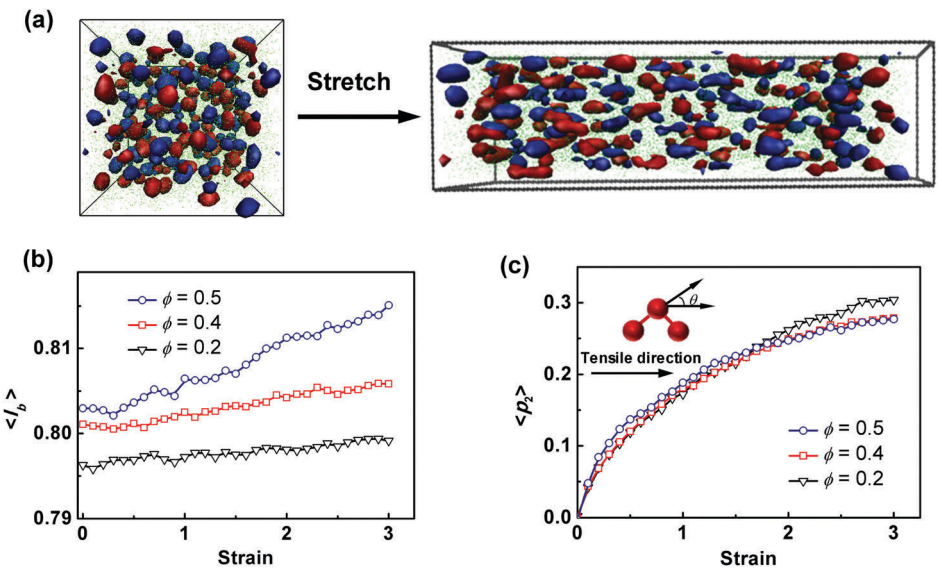

Fig. 4 (a) Structural snapshots of the systems with ϕ = 0.40 during the elongation at ε = 0 (left) and ε = 1.8 (right). (b) Average bond length $\langle l_b \rangle$ and (c) bond orientation parameter $\langle p_2 \rangle$ as a function of strain for ABC graft copolymers with various ϕ. The inset of plot (c) shows the definition of the angle θ between the bond and the tensile direction.

values with increasing strain, suggesting that the deformation is not uniform. This implies that the gels take a non-affine deformation besides the affine deformation.

To get a deeper insight into the non-affine deformation, we introduce a parameter, u, which is defined as the non-affine deviation between the real position and the affine position of tracer beads. The mean squared non-affine deviations $\langle u^2 \rangle$ for the polymer beads and the polymer chains were calculated and normalized by the affine deformation. Fig. S3b of ESI† shows the relation between the $\langle u^2 \rangle$ and the strain. It can be seen that the $\langle u^2 \rangle$ for the polymer beads is slightly larger than that for polymer chains. More importantly, the non-affine deformation is small compared to the affine deformation at a smaller strain, and thus the stress–strain relationship is linear in this regime. As the strain increases, the non-affine deformation becomes comparable to the affine deformation, leading to the non-linear stress–strain relationships at a larger strain (see Fig. 2a).

To characterize the time scale of structural relaxation, we examined the Rouse relaxation time τ_R of grafts, which is inversely proportional to the diffusion coefficient D_c. The D_c is related to the mean square displacement $(\mathrm{MSD})_t$ of grafts at time t.

$$D_c = \frac{1}{6}\lim_{t\to\infty}\frac{d}{dt}\mathrm{MSD}_t \cong {\tau_R}^{-1} \quad (5)$$

$$\mathrm{MSD}_t = \langle[\mathbf{R}_{cm}(t) - \mathbf{R}_{cm}(0)]^2\rangle \quad (6)$$

where $\mathbf{R}_{cm}(t)$ and $\mathbf{R}_{cm}(0)$ are the positions of the center-of-mass of grafts at time t and 0, respectively. For the ABC copolymer gel with $\phi = 0.40$, Fig. 5a shows the temporal evolution of the MSD_t, which is calculated from the simulations at the equilibrium state. The MSD_t of both **B** and **C** grafts increase linearly with t in the long-time-regime, suggesting that both the **B** and **C** grafts exhibit diffusive behavior. The D_c is deduced from the linear fitting of data in the long-time-regime and is equal to $0.00012\tau^{-1}$, and thus $\tau_R \cong {D_c}^{-1} = 8333.3\tau$. In addition, Fig. 5a shows that the diffusion of **C** grafts (associated by hydrogen bonds) is slower than that of the **B** grafts (not associated), suggesting that the formation of the hydrogen bonding network slows down the relaxation dynamics of **C** grafts.

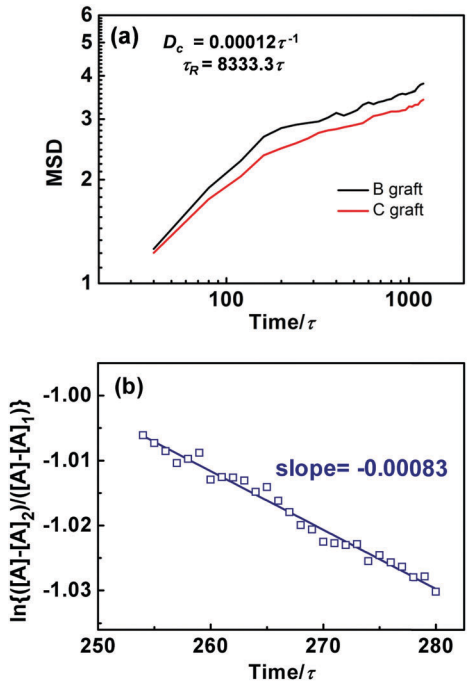

Fig. 5 (a) MSD and (b) $\ln\{([A]_t - [A]_2)/([A]_t - [A]_1)\}$ as a function of time t for the ABC graft copolymer gel with $\phi = 0.40$. The solid line in the plot (b) is the linearly fitted curve of the data, and the slope is highlighted in the plot.

In addition to the structural relaxation of solvophobic domains, the association–disassociation dynamics of hydrogen bonds also make a significant contribution to the high toughness of supramolecular gels. During the elongation process, the donor D-beads and the acceptor A-beads of hydrogen bonds in the **C** grafts can form the associated bodies A·D. Meanwhile, the A·D is able to disassociate into A and D. This association–disassociation process takes place simultaneously during the elongation process. The concentrations of A, D, and A·D satisfy the rate equations

$$\frac{d[A]_t}{dt} = -k_a[A]_t[D]_t + k_d[A\cdot D]_t \quad (7)$$

$$\frac{d[A\cdot D]_t}{dt} = k_a[A]_t[D]_t - k_d[A\cdot D]_t \quad (8)$$

where k_a and k_d are the association and disassociation rates, respectively. The $[A]_t$, $[D]_t$, and $[A\cdot D]_t$ are the number densities of acceptor A-beads, donor D-beads, and the associated body A·D at time t, respectively. The detailed derivation for the solution of rate equations is presented in Section 4 of ESI,† and the rigorous solution of rate equations is given by

$$\ln\left\{\frac{[A]_t - [A]_2}{[A]_t - [A]_1}\right\} = ([A]_1 - [A]_2)k_d\cdot K_{eq}t + \ln\left\{\frac{[A]_0 - [A]_2}{[A]_0 - [A]_1}\right\} \quad (9)$$

$$[A]_1 = -0.5\{1/K_{eq} + (1/{K_{eq}}^2 + 4[A]_0/K_{eq})^{1/2}\} \quad (10)$$

$$[A]_2 = -0.5\{1/K_{eq} - (1/{K_{eq}}^2 + 4[A]_0/K_{eq})^{1/2}\} \quad (11)$$

where the equilibrium constant K_{eq} is the ratio of k_a to k_d, the $[A]_0$ is the initial concentration of A-beads, and the variables $[A]_1$ and $[A]_2$ depend on the K_{eq} and the $[A]_0$. Taking the ABC graft copolymer gel with $\phi = 0.40$ as an example, the amounts of A, D, and A·D are respectively 182, 182, and 332, which are averaged from 20 sets of data obtained at the equilibrium state. Since the volume of the system is $27\,000{r_c}^3$, one can deduce that $[A]_e = 6.74 \times 10^{-3}\ {r_c}^{-3}$, $[D]_e = 6.74 \times 10^{-3}\ {r_c}^{-3}$, and $[A\cdot D]_e = 1.23 \times 10^{-2}\ {r_c}^{-3}$, where $[A]_e$, $[D]_e$, and $[A\cdot D]_e$ are the number densities of A, D, and A·D at the equilibrium state, respectively. According to eqn (S3), (S5), (S8) and (S9) of ESI,† we can deduce that $K_{eq} = 270.76{r_c}^3$, $[A]_0 = 0.019\ {r_c}^{-3}$, $[A]_1 = -0.011\ {r_c}^{-3}$, and $[A]_2 = 0.0047{r_c}^{-3}$. For the systems with $\phi = 0.10$, $\phi = 0.20$, and $\phi = 0.30$, the amounts of the associated body ($N_{A\cdot D,e}$), acceptor ($N_{A,e}$), and donor ($N_{D,e}$) are also obtained at the equilibrium state and used to calculate $[A\cdot D]_e$, $[A]_e$, and $[D]_e$, respectively. Table S1 of ESI† shows the values of $N_{A\cdot D,e}$, $N_{A,e}$, $N_{D,e}$, and K_{eq}

for various ϕ. When the ϕ changes, the K_{eq} maintains an approximate value around $266.87r_c^3$.

On the basis of the values of $[A]_1$ and $[A]_2$, the temporal evolution of $\ln\{([A]_t - [A]_2)/([A]_t - [A]_1)\}$ for the $\phi = 0.40$ system is shown in Fig. 5b. It can be seen that the $\ln\{([A]_t - [A]_2)/([A]_t - [A]_1)\}$ in terms of time t approximately satisfy a linear relationship, and the slope is -0.00083, which is equal to the value of $([A]_1 - [A]_2)k_d \cdot K_{eq}$ (see eqn (9)). Therefore, the disassociation rate has a value of $k_d = 2.082 \times 10^{-4}\ \tau^{-1}$. The τ_d can be estimated by the reciprocal of k_d, and thus $\tau_d = 4803.8\tau$, which is smaller than the Rouse time τ_R of 8333.3τ. This means that the relaxation time of **C** grafts is longer than the disassociation of the hydrogen bonds, implying that the network is transient and the associated **C** grafts can disassociate and re-associate many times in the Rouse relaxation time. In addition, some acceptor A-beads disassociated from A·D may re-associate with another donor D′-bead and re-form the associated body A·D′ in the Rouse relaxation time,[23] which could also cause the energy dissipation.

To further examine the dissipated energy in the elongation, we then carried out loading–unloading tests for the ABC copolymer gel with $\phi = 0.40$. In the loading process, the samples are stretched to a given loading strain ε_{load} with a tensile rate of $0.2\tau^{-1}$. In the unloading processes, the tensile force is switched off and the simulations are carried out in the *NPT* ensemble. Due to the elasticity of the gel, the elongated samples shrink, and thus the tensile strain decreases. Fig. 6a shows the mechanical hysteresis loops for the loading–unloading tests with various ε_{load} of 1.0, 3.0, 5.0, 7.0, and 8.9. Fig. 6b presents the U_{hys}–ε_{load} relationship, where the U_{hys} is defined as the area of the hysteresis loop. When $\varepsilon_{load} < 0.5$, the U_{hys} is close to zero, indicating that the gels are under elastic deformation. When $\varepsilon_{load} > 0.5$, the U_{hys} gradually increases with increasing ε_{load}, suggesting that the energy dissipation capacity of the ABC graft copolymer gel is enhanced. The appearance of mechanical hysteresis originates from the structural relaxation as well as the disassociation and re-association behaviors of hydrogen bonds. The energy is dissipated for the disassociation of the hydrogen bonds between **C** grafts, which is taken from the stress. On the other hand, when a re-association happens, the same amount of energy will be released. The released energy is dissipated through the friction of polymer chains, which is caused by the structural relaxation of solvophobic domains, the dissociation and re-association of grafts, and the slippage of polymer chains. In the equilibrium state or at low strains, the friction of polymer chains is weak, and thus the dissipated energy is small. At higher strains, the structural relaxation of solvophobic domains takes place (see Fig. 4a), and the polymer chains slip due to the orientation of the chains. As a result, the dissipated energy gradually increases. The U_{hys} as a function of ε_{load} under various polymer concentrations is shown in Fig. S4a of ESI.† It is illustrated that the U_{hys} is boosted as the ϕ increases, and thus the systems with a larger ϕ are tougher.

We then implemented the elongation–compression cycle tests for the ABC graft copolymer gel with $\phi = 0.40$. Unlike the loading–unloading tests, the gel is under compression with a rate of $-0.2\tau^{-1}$ in the cycle tests. The stress–strain relationships

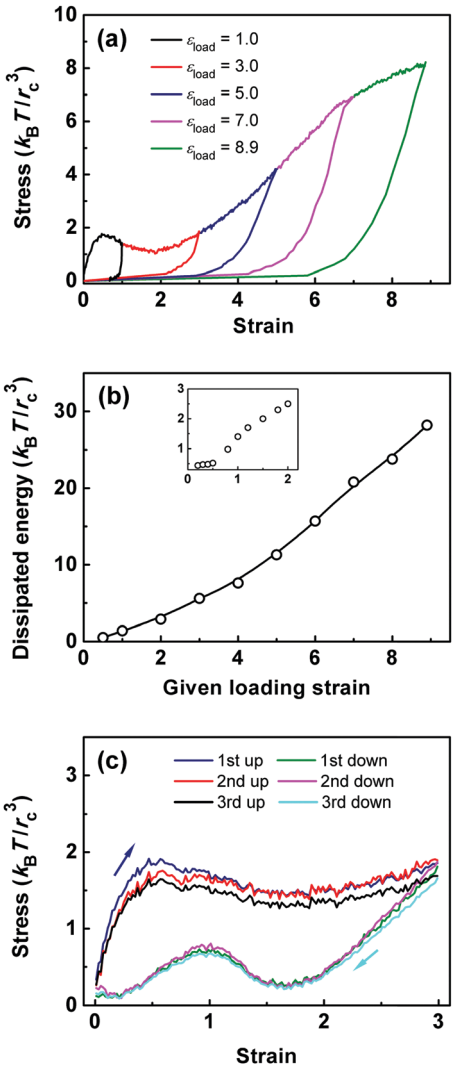

Fig. 6 (a) Stress–strain curves of the loading–unloading tests for the ABC copolymer gel with $\phi = 0.40$. (b) Dissipated energy U_{hys} as a function of the given loading strain ε_{load} in the loading–unloading tests. The inset shows the enlarged view at small ε_{load}. (c) Stress–strain curves of the elongation–compression cycle tests.

of the first three cycles are shown in Fig. 6c. In all the cycles, similar hysteresis loops are observed, suggesting that the gel has good recovery properties. In the compression processes, the stress decreases first, followed by an increase when the strain is close to 1.0, and finally decreases again (see Fig. 6c). The bump of the stress at strain $\varepsilon = 1.0$ could originate from the regeneration of the hydrogen bond energy due to the recovery of hydrogen bonds in the compression process. To verify this inference, we examined the evolution of the hydrogen bond energy in the cycle tests. Fig. S5 of ESI† shows the relationship between hydrogen bond energy and strain in the compression processes of the first three cycles. It can be seen that the hydrogen bond energy rises around $\varepsilon = 1.0$, which causes the bump around $\varepsilon = 1.0$ in the unloading curves. In addition, Fig. 6c shows that the stress values in the second and third elongation processes are slightly smaller than those in the first elongation

process, suggesting that the hydrogen bonds have not recovered completely.

Effects of the strength and directivity of hydrogen bonds on mechanical properties

As illustrated above, the hydrogen bonds play an important role in the mechanical properties of supramolecular multicompartment gels formed by ABC graft copolymers. In this subsection, we focus on the effects of the strength and directivity of hydrogen bonding interactions on the mechanical properties of ABC copolymer gels. As can be seen from eqn (2), the strength and the directivity of hydrogen bonding interactions are determined by the force constant k_A and the cutoff angle θ_c of the AHD interaction potential, respectively. Therefore, we tune these parameters to examine their influences on the mechanical properties of supramolecular gels.

Fig. 7a shows the stress–strain relations of ABC graft copolymer gels with various force constants k_A. The polymer concentration is fixed at $\phi = 0.40$ and the tensile rate is chosen as $0.2\tau^{-1}$. Four samples with $k_A = 0$, $3.0k_BT$, $5.0k_BT$, and $10.0k_BT$ were examined. Note that $k_A = 0$ means that the hydrogen bonding interactions are switched off. It was confirmed that the hydrogen bonding systems (cases of $k_A > 0$) are tougher than the system without the hydrogen bonding interaction ($k_A = 0$). In addition, the value of k_A has a more marked influence on the stress–strain relation in the large-strain-regime than that in the small-strain-regime. When the strain is small, all the samples exhibit linear elastic properties (see the inset of Fig. 7a). With the increase of k_A, the elastic modulus slightly increases, indicating that the k_A has a weak influence on the stiffness of gels. In the intermediate- and large-strain-regimes, the stress softening phenomenon becomes weak as well as the rupture stress and the elongation at break increase as the k_A increases, suggesting that the supramolecular gels are tougher in the systems with a larger k_A.

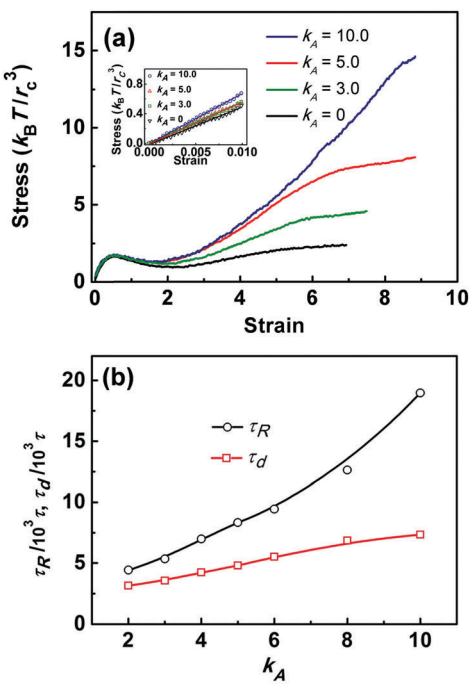

Fig. 7 (a) Stress–strain curves of the ABC graft copolymer gels with various force constants k_A. (b) The dependence of Rouse relaxation time τ_R of the grafts and the disassociation time τ_d of hydrogen bonds on the force constants k_A. The polymer concentration is fixed at $\phi = 0.40$, and the tensile rate is fixed at $0.2\tau^{-1}$.

To reveal the physical origin of the enhancement in toughness, the Rouse relaxation time τ_R and the disassociation time τ_d of hydrogen bonds were analyzed and shown in Fig. 7b. Both the τ_R and the τ_d increase with increasing k_A. As the strength of the hydrogen bonds increases, the bonding energy (see eqn (2)) is enhanced, indicating that the hydrogen bonds are more difficult to disassociate, and thus the life time of hydrogen bonds is extended (corresponding to an increase of τ_d). Therefore, the gel network is more perfect and the motion of the grafts becomes slower (corresponding to an increase of τ_R). Thus the gels become tougher and stronger, and the stress response, rupture stress, and the elongation at break increase with increasing k_A. These facts suggest that the structural relaxation is depressed as the strength of hydrogen bonding interactions increases, owing to the stronger intermolecular attraction. Meanwhile, the disassociation of hydrogen bonds slows down, *i.e.*, the τ_d increases. As a result, the gel networks turn stronger and the gels become tougher with increasing k_A. The loading–unloading tests for the systems with various values of k_A were also carried out. As shown in Fig. S4b of ESI,† the curves of U_{hys} *versus* ε_{load} imply that the gels become tougher in the systems with larger k_A.

The cutoff angle θ_c of the AHD potential is changed to examine the directivity of the hydrogen bonding interactions on the mechanical properties of the supramolecular multicompartment gels. Fig. 8a shows the stress–strain curves of the ABC graft copolymer gels with various θ_c. The polymer concentration is fixed at $\phi = 0.40$. Three samples with $\theta_c = 140^\circ$, $\theta_c = 150^\circ$, and $\theta_c = 160^\circ$ were examined. As θ_c decreases, both the rupture stress and the elongation at break grow, while the tensile modulus changes barely. As mentioned above, the hydrogen bonding interaction exists only when the θ_{AHD} is larger than θ_c. Therefore, with decreasing θ_c, more hydrogen bonds exist because the condition of $\theta_{AHD} > \theta_c$ is readily satisfied, and thus the gel network is more perfect. Fig. 8b shows the Rouse relaxation time τ_R and the disassociation time τ_d of hydrogen bonds as a function of θ_c. Both the τ_R and the τ_d are larger in the smaller θ_c systems. This suggests that the structural relaxation is depressed in the systems with a smaller θ_c, originating from the perfect network. Meanwhile, the disassociation rate of hydrogen bonds also slows down (*i.e.*, the τ_d increases). As a result, the toughness of the gel is enhanced with the decrease of θ_c. The curves of U_{hys} *versus* ε_{load} (Fig. S4c of ESI†) in the loading–unloading tests for the systems with various θ_c show that the U_{hys} is also boosted with decreasing θ_c. In addition, the elongation–compression cycle tests of systems with various k_A or θ_c are also carried out. It was found that the gels with different k_A or θ_c also show good recovery properties.

The multicompartment gel is a kind of high-performance copolymer gel, which can be achieved by introducing two or more incompatible blocks to copolymer systems. In this work, by introducing hydrogen bonding interactions to the **C** grafts, the ABC graft copolymers can form supramolecular multicompartment gels.

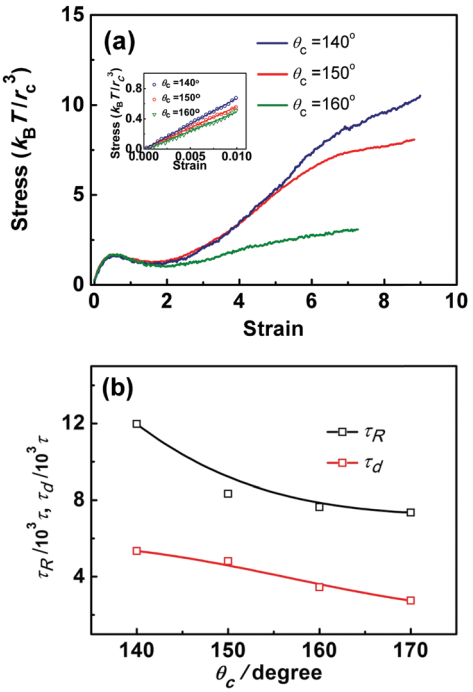

Fig. 8 (a) Stress–strain curves of the ABC graft copolymer solutions with various cutoff angles θ_c. (b) The dependence of the Rouse relaxation time τ_R of grafts and the disassociation time τ_d of hydrogen bonds on the cutoff angle θ_c. The polymer concentration is fixed at ϕ = 0.40, and the tensile rate is fixed at $0.2\tau^{-1}$.

Compared to the system without hydrogen bonding interactions, higher toughness and recovery properties are observed for the designed gels, while their stiffness remains. In addition, the 3-body AHD potential used in this work considers the directivity of hydrogen bonding interactions which is not considered in most simulations in the literature.[33,40] The results show that the directivity of the hydrogen bonds plays an important role in the mechanical properties of supramolecular multicompartment gels, and thus the mechanical properties are more controllable.

Due to the high toughness and the recovery property, the supramolecular multicompartment gels formed by ABC graft copolymers may find potential applications in biomedical technology. For instance, they can be applied as excellent injective scaffold materials. These types of injective scaffold materials can exhibit the following advantages: (1) the multicompartment gels possess enhanced and controllable toughness, which are necessary for some clinical uses, and (2) in the gels, the recoverability of gels enables the materials to self-heal under unpredictable damage, which improves the service life. Finally, we want to emphasize that our simulation results could be helpful for developing promising strategies to design gels with superior toughness, which may have applications as advanced functional materials.

Conclusions

We conceptually designed multicompartment gels formed by ABC graft copolymers with supramolecular characteristics. The dissipative dynamics simulations coupled with the non-equilibrium deformation technique was employed to study the mechanical properties of supramolecular multicompartment gels. The simulation results show that a sol–gel transition of graft copolymers takes place with increasing polymer concentration. The stress–strain curves show that the copolymer gels exhibit high toughness and recovery properties. From the microscopic origin, the high toughness originates from the structural relaxation and the association–disassociation dynamics of the hydrogen bonding interaction, which are determined by the Rouse relaxation time of grafts and the disassociation time of hydrogen bonds. Additionally, it was found that the toughness of supramolecular multicompartment gels increases with increasing the strength of the hydrogen bonding interaction or decreasing their cutoff angle, while the stiffness is maintained. These findings reveal the microscopic origin of distinct mechanical properties of graft copolymer gels, which provide useful information for designing high-performance gels based on complex topology macromolecules.

Conflicts of interest

There are no conflicts of interest to declare.

Acknowledgements

This work was supported by the National Natural Science Foundation of China (No. 21474029 and 51621002). Support from the Projects of Shanghai municipality (No. 16520721900 and 14DZ2261205) and the Fundamental Research Funds for the Central Universities (No. 222201817021) is also appreciated.

Notes and references

1 C. Sanchez, H. Arribart and M. M. G. Guille, *Nat. Mater.*, 2005, **4**, 277–288.
2 W. H. Binder, L. Petraru, T. Roth, P. W. Groh, V. Pálfi, S. Keki and B. Ivan, *Adv. Funct. Mater.*, 2007, **17**, 1317–1326.
3 J. Li, J. A. Viveros, M. H. Wrue and M. Anthamatten, *Adv. Mater.*, 2010, **19**, 2851–2855.
4 A. Noro, M. Hayashi and Y. Matsushita, *Soft Matter*, 2012, **8**, 6416–6429.
5 S. Seiffert and J. Sprakel, *Chem. Soc. Rev.*, 2012, **41**, 909–930.
6 L. Voorhaar and R. Hoogenboom, *Chem. Soc. Rev.*, 2016, **45**, 4013–4031.
7 T. Narita and T. Indei, *Macromolecules*, 2016, **49**, 4634–4646.
8 P. Cordier, F. Tournilhac, C. Soulie-Ziakovic and L. Leibler, *Nature*, 2008, **451**, 977–980.
9 Q. Chen, C. Huang, R. A. Weiss and R. H. Colby, *Macromolecules*, 2015, **48**, 1221–1230.
10 J. Hao and R. A. Weiss, *Macromolecules*, 2016, **49**, 6687–6693.
11 K. Kojio, M. Furukawa, S. Motokucho, M. Shimada and M. Sakai, *Macromolecules*, 2009, **42**, 8322–8327.
12 P. Song, Z. Xu and Q. Guo, *ACS Macro Lett.*, 2013, **2**, 1100–1104.

13 Y. F. Yue, M. A. Haque, T. Kurokawa, T. Nakajima and J. P. Gong, *Adv. Mater.*, 2013, **25**, 3106–3110.
14 M. Guo, L. M. Pitet, H. M. Wyss, M. Vos, P. Y. Dankers and E. W. Meijer, *J. Am. Chem. Soc.*, 2014, **136**, 6969–6977.
15 X. Li, T. Kurokawa, R. Takahashi, M. A. Haque, Y. Yue, T. Nakajima and J. P. Gong, *Macromolecules*, 2015, **48**, 2277–2282.
16 G. Song, Z. Zhao, X. Peng, C. He, R. A. Weiss and H. Wang, *Macromolecules*, 2016, **49**, 8265–8273.
17 M. J. Serpe and S. L. Craig, *Langmuir*, 2007, **23**, 1626–1634.
18 C. L. Lewis, K. Stewart and M. Anthamatten, *Macromolecules*, 2014, **47**, 729–740.
19 E. M. Foster, E. E. Lensmeyer, B. Zhang, P. Chakma, J. A. Flum, J. J. Via, J. L. Sparks and D. Konkolewicz, *ACS Macro Lett.*, 2017, **6**, 495–499.
20 T. T. T. Myllymäki, L. Lemetti, Nonappa and O. Ikkala, *ACS Macro Lett.*, 2017, **6**, 210–214.
21 J. Cui and A. del Campo, *Chem. Commun.*, 2012, **48**, 9302–9304.
22 M. Rubinstein and A. N. Semenov, *Macromolecules*, 2001, **34**, 1058–1068.
23 A. N. Semenov and M. Rubinstein, *Macromolecules*, 2002, **35**, 4821–4837.
24 L. Brunsveld, B. J. B. Folmer, E. W. Meijer and R. P. Sijbesma, *Chem. Rev.*, 2001, **101**, 4071–4097.
25 S. Hackelbusch, T. Rossow, P. van Assenbergh and S. Seiffert, *Macromolecules*, 2013, **46**, 6273–6286.
26 T. Rossow, A. Habicht and S. Seiffert, *Macromolecules*, 2014, **47**, 6473–6482.
27 F. Meng, R. H. Pritchard and E. M. Terentjev, *Macromolecules*, 2016, **49**, 2843–2852.
28 T. Yan, K. Schröter, F. Herbst, W. H. Binder and T. Thurn-Albrecht, *Macromolecules*, 2017, **50**, 2973–2985.
29 L. Zhang, J. Lin and S. Lin, *Soft Matter*, 2009, **5**, 173–181.
30 X. Zhu, L. Wang and J. Lin, *Macromolecules*, 2011, **44**, 8314–8323.
31 L. Guo and E. Luijten, *J. Polym. Sci., Part B: Polym. Phys.*, 2005, **43**, 959–969.
32 R. S. Hoy and G. H. Fredrickson, *J. Chem. Phys.*, 2009, **131**, 224902.
33 Z. Li, H. Djohari and E. E. Dormidontova, *J. Chem. Phys.*, 2010, **133**, 184904.
34 B. Qiao, X. Zhao, D. Yue, L. Zhang and S. Wu, *J. Mater. Chem.*, 2012, **22**, 12339–12348.
35 E. Hajizadeh, B. D. Todd and P. J. Daivis, *J. Chem. Phys.*, 2014, **141**, 194905.
36 J. Castillo-Tejas, S. Carro and O. Manero, *ACS Macro Lett.*, 2017, **6**, 190–193.
37 C. Ma, H. Wu, Z.-H. Huang, R.-H. Guo, M.-B. Hu, C. Kubel, L.-T. Yan and W. Wang, *Angew. Chem., Int. Ed.*, 2015, **54**, 15699–15704.
38 Y. Han and W. Jiang, *J. Phys. Chem. B*, 2011, **115**, 2167–2172.
39 Y. Han, J. Cui and W. Jiang, *J. Phys. Chem. B*, 2012, **116**, 9208–9214.
40 M. Wilson, A. Rabinovitch and A. R. C. Baljon, *Macromolecules*, 2015, **48**, 6313–6320.
41 D. Amin, A. E. Likhtman and Z. Wang, *Macromolecules*, 2016, **49**, 7510–7524.
42 H. Wang, C. Junghans and K. Kremer, *Eur. Phys. J. E: Soft Matter Biol. Phys.*, 2009, **28**, 221–229.
43 Y. R. Sliozberg, J. W. Andzelm, J. K. Brennan, M. R. Vanlandingham, V. Pryamitsyn and V. Ganesan, *J. Polym. Sci., Part B: Polym. Phys.*, 2010, **48**, 15–25.
44 M. Yue, Y. Li, Y. Hou, W. Cao, J. Zhu, J. Han, Z. Lu and M. Yang, *ACS Nano*, 2015, **9**, 5807–5817.
45 G. Kacar and G. de With, *Phys. Chem. Chem. Phys.*, 2016, **18**, 9554–9560.
46 J. Kwak, S. S. Nam, J. Cho, E. Sim and S. Y. Lee, *Phys. Chem. Chem. Phys.*, 2017, **19**, 10274–10281.
47 T. Jiang, L. Wang and J. Lin, *Langmuir*, 2013, **29**, 12298–12306.
48 G. Xu, Z. Huang, P. Chen, T. Cui, X. Zhang, B. Miao and L.-T. Yan, *Small*, 2017, **13**, 1603155.
49 P. Xu, J. Lin, L. Wang and L. Zhang, *J. Chem. Phys.*, 2017, **146**, 184903.
50 S. I. Mayo, B. D. Olafson and W. A. Goddard III, *J. Phys. Chem.*, 1990, **94**, 8897–8909.
51 R. D. Groot and P. B. Warren, *J. Chem. Phys.*, 1997, **107**, 4423–4435.
52 J. Li, J. A. Viveros, M. H. Wrue and M. Anthamatten, *Adv. Mater.*, 2007, **19**, 2851–2855.
53 Y. Liu, V. S. Bryantsev, M. S. Diallo and W. A. Goddard III, *J. Am. Chem. Soc.*, 2009, **131**, 2798–2799.
54 S. Plimpton, *J. Comput. Phys.*, 1995, **117**, 1–19.
55 T. Jiang, L. Wang and J. Lin, *RSC Adv.*, 2014, **4**, 35272–35283.
56 J. Liu, S. Wu, L. Zhang, W. Wang and D. Cao, *Phys. Chem. Chem. Phys.*, 2011, **13**, 518–529.
57 D. R. Rottach, J. G. Curro, G. S. Grest and A. P. Thompson, *Macromolecules*, 2004, **37**, 5468–5473.
58 J. Gao and J. H. Weiner, *J. Chem. Phys.*, 1995, **103**, 1614–1620.
59 J. Liang, G. Shan and P. Pan, *Soft Matter*, 2017, **13**, 4148–4158.
60 Q. Chen, L. Zhu, L. Huang, H. Chen, K. Xu, Y. Tan, P. Wang and J. Zheng, *Macromolecules*, 2014, **47**, 2140–2148.

